Testing low/very low frequency acoustic sources for basin-wide propagation in the Indian Ocean

Donna K. Blackman[a] and Catherine de Groot-Hedlin
Scripps Institution of Oceanography, La Jolla, California 92093

Phil Harben
Lawrence Livermore National Labs, Livermore, California 94550

Allan Sauter and John A. Orcutt
Scripps Institution of Oceanography, La Jolla, California 92093

(Received 29 August 2003; revised 2 June 2004; accepted 9 July 2004)

Low/very low frequency acoustic signals were transmitted to distant receivers in the Indian Ocean. The aim was to test methods for characterizing the hydroacoustic capability of the International Monitoring System (IMS) that discriminates for nuclear tests in the region. Several acoustic sources were deployed between Seychelles and Fremantle, Australia, and the IMS receivers comprised a network of hydrophones off Diego Garcia and Australia. Two of the three acoustic sources tested produced basin-scale propagation of impulsive signals. Single glass spheres imploded within the sound channel produced a clear signal at frequencies above ~40 Hz, at ranges of hundreds to a thousand kilometers. Five-sphere glass implosions were recorded at ranges up to 4400 km. Near-sea surface shots from a large airgun array were recorded in several cases at ranges of hundreds to thousands of kilometers, the frequency of the highest signal-to-noise ratio arrivals varied within the 5–100 Hz band. High background noise level was a key factor at IMS stations that did not detect the airgun signals in the 5–15 Hz band. In a few cases, details of bathymetric features that are not well represented in the digital elevation model contributed to unexpected variation in relative signal levels between IMS stations. [DOI: 10.1121/1.1786711]

PACS numbers: 43.30.Qd [WLS] Pages: 2057–2066

I. INTRODUCTION

Hydroacoustic monitoring for nuclear explosions in the Indian Ocean is a goal for which detailed testing is still under way. The signal from a large acoustic source in the Indian Ocean basin would almost certainly be detected by the monitoring hydrophones, if not directly then via reflections off topographic slopes behind blocked areas (Pulli *et al.*, 1999; Hanson *et al.*, 2002). The challenge is to accurately determine the location of the source and to discriminate between natural, legitimate manmade, or clandestine nuclear explosion causes for the signal, so that appropriate response is undertaken (Hanson *et al.*, 2001).

Determination of a hydroacoustic source location depends on models of both sound propagation within the ocean and seafloor topography, which can attenuate the signal as it travels along the path between source and receiver. Differences in oceanographic properties (temperature, salinity) result in variable sound speed structure and this affects the travel time of acoustic signals. For basin-wide propagation, the low velocity ''sound channel'' is responsible for minimizing losses to allow detection of very distant sources. Signals that propagate along paths where topographic features protrude into the sound channel, or where the source or receiver is near a continental shelf or slope, lose energy due to partitioning of phases at the seafloor interface. Diffraction and scattering at topographic features can alter the path and contribute to complexity in the wave form that is recorded at a receiver. Therefore, models of propagation and loss employed in event location and characterization of an unknown source depend on databases of oceanic properties and topography. The required resolution of these databases, particularly the topography, is one of the things that remain to be determined for the Indian Ocean International Monitoring System (IMS). In addition, while recent modeling techniques are able to incorporate most aspects of underwater sound propagation and loss, there is a trade-off between the level of modeling complexity and the resources required for the calculation. For real-time monitoring, one would like to minimize the computational effort while retaining sufficient accuracy to obtain results within the desired limits. One way to assess which factors control variability in the acoustic propagation/losses for one region versus another is to transmit a known source signal from various locations within an ocean basin. Differences in the recorded signal between stations can guide plans for additional mapping to enhance the database or efforts to refine numerical modeling approach.

A fundamental question arises when undertaking to quantitatively assess the resolution of databases employed in very low/low frequency (VLF/LF) sound propagation models within an ocean basin—what acoustic sources can provide the information needed while ensuring a feasible series of experiments? Human and marine mammal safety is a key concern and regulation of international shipping and handling of explosives is another difficulty. We deployed two types of sources that were nonexplosive. Small implosives

[a]Author to whom correspondence should be addressed; electronic mail: dblackman@ucsd.edu

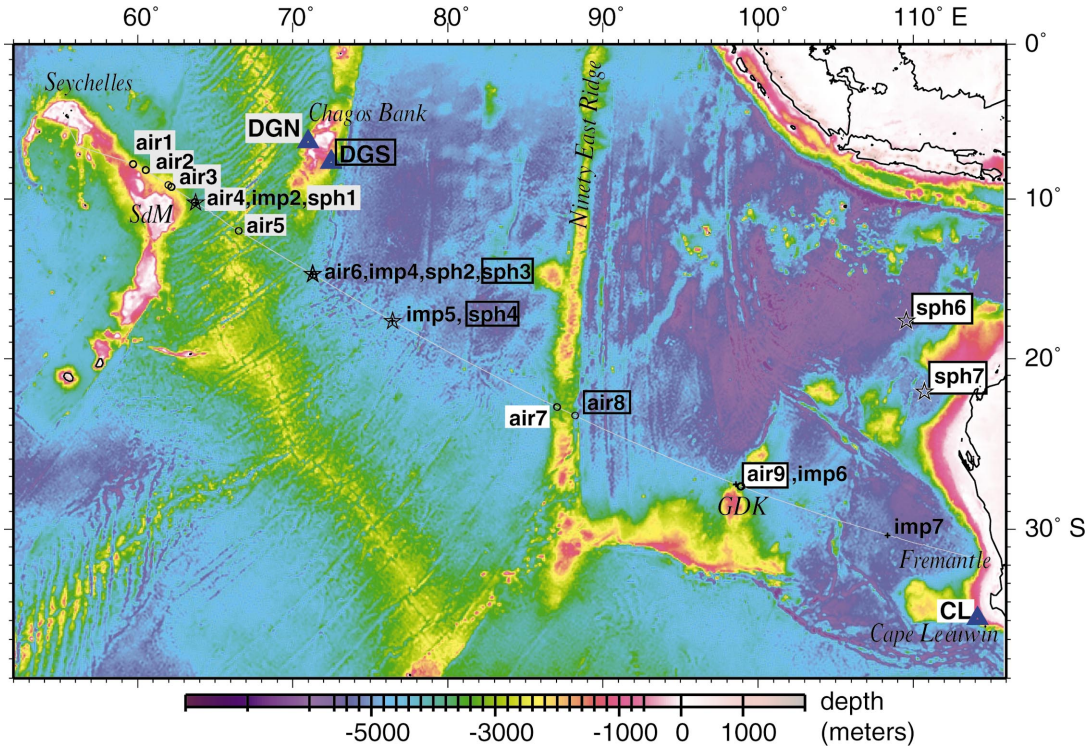

FIG. 1. Topographic model of Smith and Sandwell (1997) in the Indian Ocean region is overlain by 2001 R/V EWING shiptrack (gray line) and the acoustic source locations for our experiment. Yellow-red colors illustrate shallow bathymetric features that attenuate signals propagating in the sound channel across the basin. IMS hydrophone stations are shown by blue triangles. Circles show where the airgun array shooting (*air*) was conducted. Stars show glass sphere (*sph*) implosion stations and five-sphere implosions are highlighted in white. Crosses are where the MPL/SIO imploding cylinder (*imp*) was fired. Gray-fill boxes indicate sources observed at IMS hydrophones at Diego Garcia, north (DGN), black-outline boxes indicate sources observed at Diego Garcia, south, (DGS), and white-fill boxes show sources observed at Cape Leeuwin (CL). SdM indicates Saya de Malha bank; GDK is Gulden Draak Knoll.

were fired as single-shots in the water column at depths of 300–1200 m. The other source type was a large airgun array, such as is commonly employed for marine seismic reflection surveys conducted by oil industry and academic researchers. This system was fired repeatedly near the sea surface (9–12 m depth) at selected source sites.

Our work in the Indian Ocean took advantage of available shiptime in 2001 and a sparse network of hydrophones that are part of the IMS overseen by the Comprehensive Test Ban Treaty Office of the United Nations. The research ship R/V EWING departed Mahe Island, Seychelles, and steamed essentially a great circle path to Fremantle, Australia. During the 18-day cruise, the Ewing's airgun array was used nine times and implosive sources were deployed twelve times, of which nine successfully fired (Fig. 1). During the following cruise off northwest Australia, two additional, larger, implosive sources were successfully fired.

The results reported here are initial steps toward the overall goal of fully characterizing the influence on acoustic propagation throughout the Indian Ocean Basin of topographic blockage, diffraction, and scattering, and oceanographic complexities such as the high temperature and salinity gradients near the Antarctic Convergence. We have determined the range over which small and moderate sized implosive signals (Secs. III A and III B) will propagate with sufficiently low loss to be detected at distant hydrophones (Sec. III C). In addition, we discuss the relationship between near-source seafloor topography (Secs. IV B and V) and the efficiency of coupling acoustic energy from near-sea surface sources (Sec. IV A) into the sound channel for subsequent basin-scale propagation. We assess the accuracy with which the recorded airgun array signals can be used to calculate the location of near-sea surface sources (Sec. IV C). Finally, the differences between expected losses and the level of the observed signal-to-noise ratio for different source-receiver paths are noted (Sec. V) and possible causes for the difference are discussed.

II. RECEIVERS

A. IMS hydrophones

The hydrophone stations of the International Monitoring System that were operating in the Indian Ocean in late 2001 are located near Diego Garcia and off Cape Leeuwin, southwestern Australia (Fig. 1). The two stations in the vicinity of Diego Garcia—DGN and DGS—are each comprised of 3 hydrophones deployed 1–2 km apart. DGN hydrophones are deployed at water depths of 1180–1250 m on the western slope of the Chagos Bank, on which the island of Diego Garcia is located. The instruments for DGS are at water depths of 1350–1415 m on the eastern slope of Chagos Bank. The Cape Leeuwin (CL) hydrophones are deployed at water depths of 1045–1065 m. Digital data are recorded at 250 samples/s and the instrument response dictates useful data for our analyses in the 2–100 Hz band.

The background noise levels are different at the three IMS hydrophone stations (Fig. 2). During our October cruise, the southwest monsoon ensured steady head winds

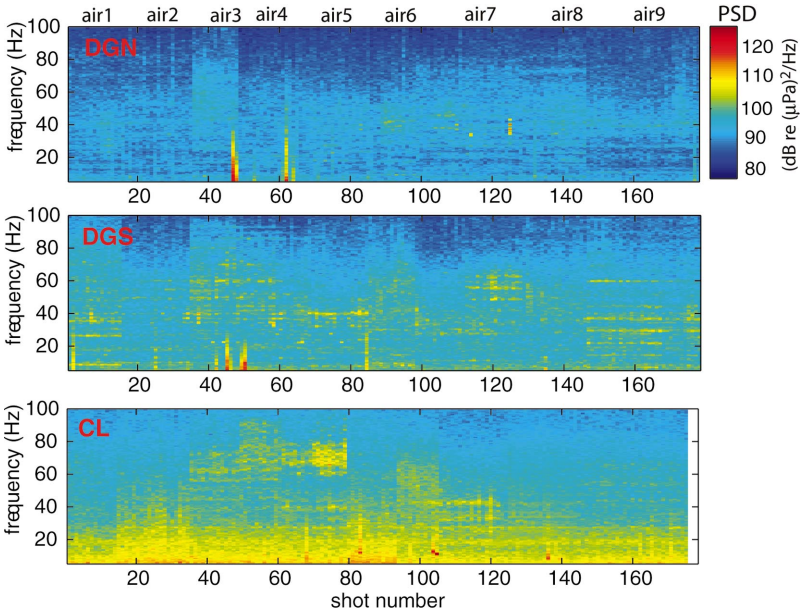

FIG. 2. Noise levels at the IMS stations during the times of airgun array shooting. Spectragrams show 10 s window that immediately precedes each shot using data taken from a representative sensor at each station. Note that time is not continuous along the horizontal axis (see Table I and Fig. 1). The shooting sites are labeled at top.

and seas from the east that, in combination with swell traveling from the Southern Ocean, resulted in higher noise at DGS than at DGN. Cape Leeuwin background noise levels varied the most but were consistently higher than DGS during our study. This reflects storms and generally high sea states in the Southern Ocean. A series of distant earthquakes briefly increased the background levels on several days at Diego Garcia (for example, during *air3* shots 45–48, jd 281).

B. Near-source hydrophone

A calibrated hydrophone was deployed from the ship's deck to document the near-source signal for each implosion and a few representative airgun array shots. Source location and time, accurate to a second, were obtained from shipboard GPS data. More detailed timing was obtained from the near-source hydrophone data. The arrival times of the direct and sea surface reflected signals recorded by the hydrophone were picked with a precision of 0.001 s and the time difference between the two phases was used to determine the depth of the hydrophone, using a local water velocity profile. The depth of the implosive source was determined from the wire-out reading on the winch and was usually accurate to within a meter or two. Spectral estimates are too noisy to provide independent confirmation of implosion depth at meter-scale resolution. The average local velocity for the depth interval between the hydrophone and the source was used to compute the absolute source time by differencing from the direct arrival time at the hydrophone. The signal level was corrected back to a 1 m distance from the source assuming linear decrease of pressure with radial distance from a point source. The overall uncertainty of the implosive source time, considering all these factors, is typically ± 0.01 s.

III. IMPLOSIONS

A. LLNL imploding glass spheres

Imploding sources have a relatively long history of use (Isaacs and Maxwell, 1952; Orr and Shoenberg, 1976). Recent work shows that they can be made reliable and can be designed to produce a signal that is adequate for long-range calibration (Sauter and Dorman, 2003; Harben *et al.*, 2000). Two versions of glass sphere imploding sources were employed for our experiment—a single-sphere and a five-sphere device (Harben *et al.*, 2000; Harben and Boro, 2001). The single 22 l glass sphere implodes when a piston driven smashing system triggers at a predetermined depth through failure of a rupture disk. The five-sphere device uses the same piston driven smashing system to break a central sphere. The surrounding four spheres fail as a direct result of the first one. The single sphere produces a signal [Fig. 3(a)] with an initial, relatively low frequency rarefactional pulse that corresponds to the inrush of water caused by failure of the glass container. Convergence at the sphere center is the instant of shock wave formation, giving rise to the spike that

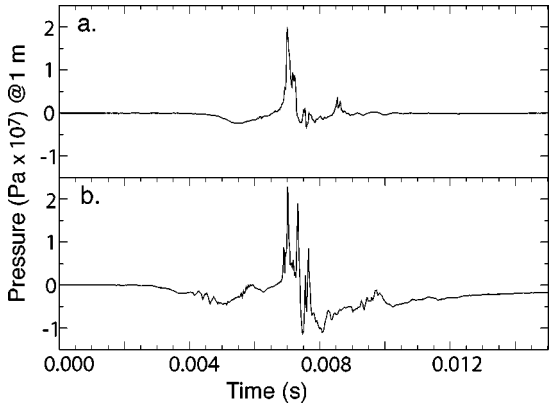

FIG. 3. Near-source recording of glass sphere implosions at 680 m depth, corrected to 1 m range from the shots. (a) Single glass sphere implosion; (b) five-sphere implosion.

dominates the record; a small bubble pulse follows. The record in Fig. 3(b) shows a composite collapse of five spheres during the initial rarefactional pulse of the wavetrain. Short duration features riding on the longer rarefactional pulse are consistent for both of the five-sphere source wave forms we recorded but the reasons for these features are not clear. The shock wave from the first implosion is visible, overlain, and followed by the implosion shock waves from the other spheres. The number and pattern of these spikes were significantly different for the two five-sphere source records. The time differences are consistent with failure caused by fracture propagation from sphere to sphere but are not consistent with a shock wave driven by collapse of adjacent spheres from the first implosion.

The imploding glass spheres achieve maximum levels in the 300–500 Hz range of 250–270 dB *re* 1 μPa, corrected back to 1 m from the source, but the level at other frequencies is much reduced. At the source, the pulse is about 6 ms long.

B. MPL/SIO wireline imploder

The 20 l, cylindrical configuration of the MPL/SIO imploder (Sauter and Dorman, 2003) produces a signal whose level in the 100–200 Hz band is 5–10 dB lower than the single glass sphere signal. We were not able to recognize any of the imploder shots in the IMS hydrophone data.

C. IMS hydrophone recordings

Five of the six successful imploding glass sphere shots were detected at IMS hydrophone stations (Fig. 1). Three were single sphere implosions, recorded at Diego Garcia, and two were five-sphere implosions, recorded at both Diego Garcia and at Cape Leeuwin. All detected shots had source depth ~680 m; a 320 m deep implosion (*sph2*) fired at the same location as a deeper shot (*sph3*) was not detected. Ranges between the single-sphere shots and the receiver were 800–1200 km. The single sphere signal level rises above the noise level for frequencies greater than about 40 Hz (Fig. 4). The duration of the received signal is quite a bit longer than the near-source pulse at almost 400 ms.

The bandwidth of the five-sphere arrivals is similar to that of the single-sphere recordings. Peak amplitudes are not right at the onset of the arrival but are consistently in front of the center of the envelope whose length is about 1 s (Fig. 5). The five-sphere implosions were conducted along the western Australia continental margin with ranges to Diego Garcia of 4168 km (*sph6*) and 4397 km (*sph7*) and ranges to Cape Leeuwin of 1960 and 1465 km (Fig. 1).

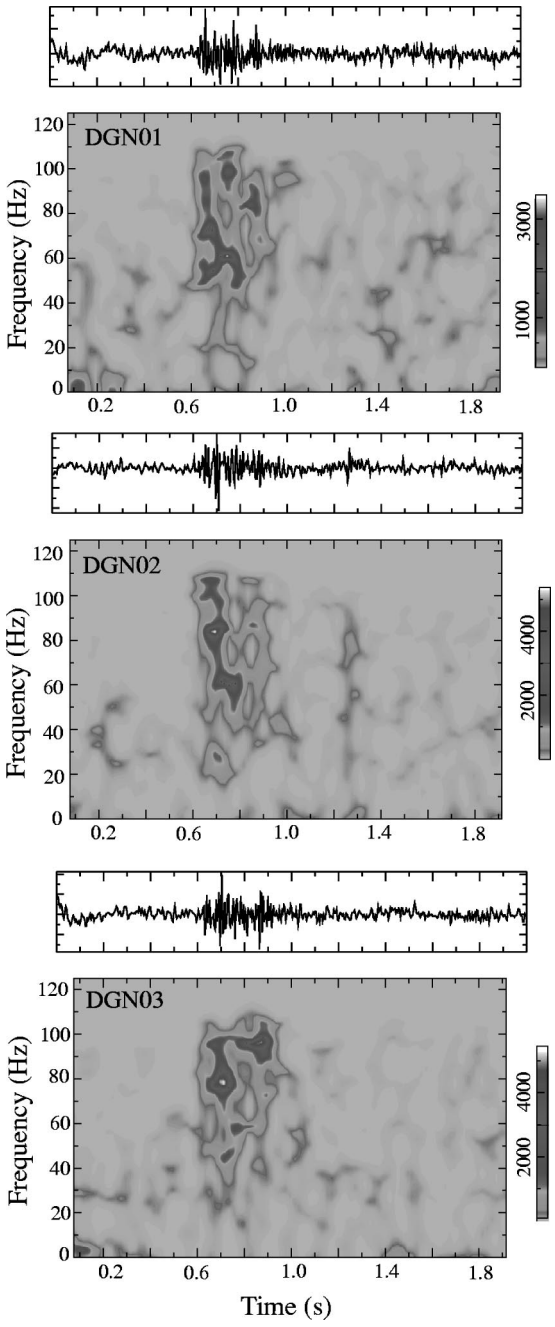

FIG. 4. Spectragrams of the signal from single-glass-sphere implosion *sph1* recorded at each sensor of station DGN. Note the short signal duration and concentration of energy at frequencies above 40 Hz. Unfiltered time sections are above each spectragram (instrument counts, grayshade, show relative level of signal and noise). Time zero corresponds to travel-time at 1.49 km/s for range of 798 km to DGN01.

IV. AIRGUN ARRAY SHOTS

A. Source

The R/V EWING array of 20 airguns with a total volume of 8465 cubic inches was used.[1] Each of our shooting periods lasted about 30 min, and shot interval varied from 57 to 173 s. Ship speed during the shooting was ~4 knots. The peak level of the airgun array signal was measured at 230–240 dB *re* 1 μPa (adjusted to 1 m range) in the 5–60 Hz range (Fig. 6). The duration of the airgun array pulse is about 12 ms. Source depth for the airgun array shots is 9–12 m and the details for each shooting site are listed in Table I.

Shot trigger times are generally accurate to a millisecond. Shot locations generally are accurate to about 10 m; loss of high resolution (P Code) GPS during the last shooting period resulted in greater uncertainty, ~50 m. Corrections for the difference in location between the GPS receiver and the center of the airgun array are incorporated in the airgun shot locations listed in Table I.

Seafloor topography in the vicinity of each shot controls

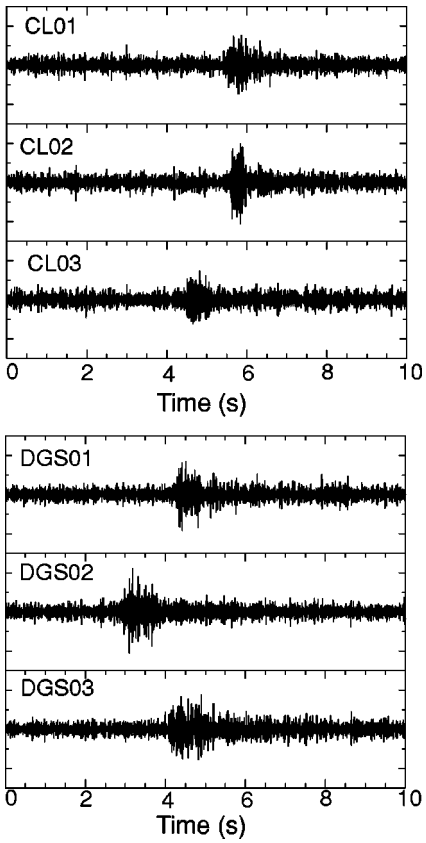

FIG. 5. Recordings of the five-sphere glass ball implosion (*sph7*) at distant IMS hydrophones. Cape Leeuwin time series are shown in the top panels and are high pass filtered with corner at 40 Hz; Diego Garcia station DGS time series are shown in the lower panels with the same filter applied. Time zero corresponds to travel time at 1.49 km/s for range of 4396 and 1465 km to DGS01 and CL01, respectively.

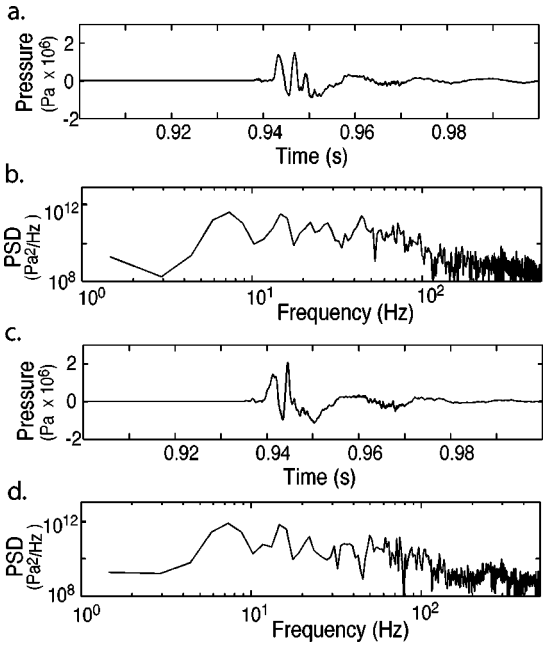

FIG. 6. Time series (a), (c) and power spectral density (b), (d) of two representative airgun array shots as recorded on the near-source hydrophone. Levels are corrected to a distance of 1 m from the source. The source signature is quite consistent in the 5–25 Hz band, with levels differing by less than a few decibels between shots. Variability that occurs in the 25–100 Hz band is illustrated by these two shots.

the efficiency of coupling the airgun energy into a nearly horizontally propagating wave that is guided long distance by the sound channel. Details of the local depth, slope, and seafloor roughness all contribute to this process of transferring energy from the dominantly down-going pulse[1] into horizontally traveling rays.

B. IMS hydrophone recordings

The signal recorded for our series of airgun shooting sites varied as a function of both receiver and source location. Some of this variability was expected as blockage or near-source seafloor conditions changed, but in some cases the increase or decrease in SNR between sites/stations was surprising. Chagos bank blocked propagation to DGS for the first four airgun sites. We expected CL to be blocked from the first site by the Saya de Malha bank and from some of the subsequent five sites, by the Ninety East Ridge (Fig. 1). Propagation from shooting sites *air6–air9* to DGN was blocked by the Chagos bank.

Figures 7–9 illustrate the difference in arrival character between airgun shooting sites and between receiving stations. The records for the source–receiver pairs shown in Figs. 7 and 8(a)–(c) have sufficiently high SNR that the individual shots are visible in filtered sections. Stacking of all shots for a given site, following moveout correction (a time shift that takes into account the small difference in source–receiver range due to ship motion during shooting), increases the SNR of the main arrival and retains features common to the 5–10 Hz bandpassed wave form for the entire shooting period; this is what is shown in Fig. 8. Stacking is ineffective for frequencies greater than 30 Hz; we infer that in this band acoustic energy is more strongly influenced by details of the seafloor topography. The seafloor changes somewhat as the ship progresses along the track within a single site (Fig. 10; ship position cannot be held when the airguns are deployed/firing), so details of the wave form can vary. The recordings of *air2* shots have high SNR in the 5–10 Hz range and the time series data show that the wave train following the initial pulse is short [$\sim$2 s; Fig. 8(a)]. The *air5* shots have high SNR in the 5–40 Hz band [Fig. 7(a)] and the wave duration after the main pulse exceeds 5 s in the 5–10 Hz band [Fig. 8(b)]. Although both had good SNR, transmission loss between the airgun source and the receivers was significantly lower for *air5* shots than for *air2* shots (Fig. 9).

Both DGS and CL recorded the shots for *air9* [Figs. 8(c), 8(d), Fig. 9]. In the 40–60 Hz range, DGS recordings exceed the noise level significantly but the wave forms are not very similar, therefore stacking does not significantly improve SNR. In the 5–10 Hz band, the stacked DGS wave forms are somewhat consistent between the individual hydrophones, showing a narrow peak about 3 s from the onset of the arrival [Fig. 8(c)]. At CL, the record contains significant energy in a broader frequency band for the *air9* shots—30–60 Hz (Fig. 9). The *air9* signals are not discernible in the individual shot records in the 5–10 Hz range, however the arrival is apparent in the stacked section [Fig. 8(d)] where SNR is 2 or less. The stacked *air9* wave forms are not consistent between the individual CL hydrophones.

TABLE I. Airgun array shot lines (start/end).[a]

jd hr:mn	Lat (S)	Ion (E)	Seafloor	Interval	Site	Shot No.
280 19:14	7°46.1′	59°41.6′	2110 m	97 sec	air1	1–9
280 19:27	7 46.2	59 42.5	2145			
280 19:33	7 46.3	59 42.9	2205	173		11–14
280 19:42	7 46.5	59 43.4	2270			
281 02:38	8 8.5	60 30.7	2575	127	air2	22–35
281 03:03	8 9.5	60 32.1	2655			
281 16:48	9 13.7	62 09.8	2645	173	air3	36–46
281 17:17	9 14.7	62 11.5	2720			
282 05:22	10 12.2	63 40.9	3540	57	air4	49–59
282 05:31	10 12.6	63 41.6	3530			
282 05:38	10 12.7	63 41.8	3520	173		61–68
282 05:58	10 13.4	63 42.8	3660			
283 04:33	12 01.8	66 30.6	2965	127	air5	69–83
283 05:03	12 02.6	66 32.2	3330			
284 15:34	14 48.3	71 19.5	4850	173	air6	86–96
284 16:03	14 49.5	71 20.8	4875			
289 02:11	22 55.5	87 02.8	3370	127	air7	99–114
289 02:43	22 54.6	87 00.7	3455			
289 02:45	22 54.6	87 00.7	3445	57		115–128
289 02:58	22 54.3	87 00.0	3550			
289 12:28	23 25.0	88 11.3	2985	173	air8	129–139
289 12:57	23 25.6	88 13.3	3240			
289 12:59	23 25.6	88 13.5	3235	57		140–146
289 13:04	23 25.7	88 13.9	3105			
292:02:10	27 33.2	98 51.6	2710	57	air9	147–170
292:02:32	27 33.7	98 53.0	2800			
292:02:35	27 33.8	98 53.2	2810	127		171–178
292:02:46	27 34.0	98 53.9	2845			

[a]Detailed listing of individual shots available at AIP online archive.

All of the airgun array shots to the west of DGN (*air1–air5*) were visible in the recordings at that site (Fig. 9). The transmission loss was lowest in the 5–25 Hz band for *air5* shots, which were both the closest and had least blockage. A consistent, 5–10 dB lower signal level was observed in DGN recordings for shooting periods *air1–air4* in this VLF band. This difference is several decibels greater than is expected solely based on the difference in range (3 dB). In the 50–100 Hz band, *air1* had the lowest transmission loss at DGN. This site had the shallowest (1900–2200 m) depths and a steady NNE slope. No clear signals of shots *air6–air9* were evident at DGN.

Signal levels exceed noise by several decibels for airgun array shots observed at DGS from sites to the east (*air8–air9*, greater loss at *air7*; Fig. 9). The closest unblocked site (*air6*) did not produce signals at DGS due to deep and dominantly smooth seafloor [Fig. 10(c)] that cannot effectively entrain energy into the sound channel. The signal from *air9* recorded at DGS is clearly visible at a whole-basin-scale source–receiver range of about 4825 km.

The only shots that were clearly visible in the VLF band at Cape Leeuwin were the shots of *air9*, at a range of 1665 km. Blockage of *air8* shots is not known to be significant and CL noise levels during those shots were similar to levels during the *air9* shots so it is not clear why these shots were not observed. The *air7* shots occurred during a somewhat noisier period (Fig. 2) and over the west-dipping slope of the Ninety East Ridge that was not as favorable for entrainment in the sound channel in the direction of CL. However, some energy did propagate the full range. Calculated transmission loss for *air7* is similar to that for *air9* in the 20–90 Hz band where signal was more than 3 dB above background noise (Fig. 9).

C. Determination of near-sea surface source location

None of our shots were recorded at all three stations so we cannot triangulate, in the classic sense, to determine the location of the source. However, beam-forming provides constraints on the back-azimuth when the SNR is sufficiently high in the 5–10 Hz band. Attempts at beam-forming for higher frequencies were not productive. In the time domain, uncertainty in relative hydrophone location ($\sim$10 m, Lawrence, 2003, corresponding to 1/15th of a wavelength at 10 Hz) degrades results from the cross correlation at higher frequency. The spectral estimates are not robust enough above 10 Hz to allow beaming in this domain. Only DGN had sufficiently high SNR in the 5–10 Hz band. Back-azimuths, computed by cross correlating arrivals over 10 s windows at this station have mean errors of 0.45° for *air1–air4*, for all shots with a SNR larger than 1.5. This uncertainty in back-azimuth would yield a location uncertainty of 6–10 km at the shot ranges (known here, which would not be the case for a clandestine test), which vary from 800 to 1260 km.

The cross-correlation estimates of the back-azimuths at DGN for the *air5* sequence were off by as much as 30°, even though the SNR was high in the 5–10 Hz band. This most likely is due to the lengthy coda observed for these shots. As an alternate approach, we determined the azimuth by picking

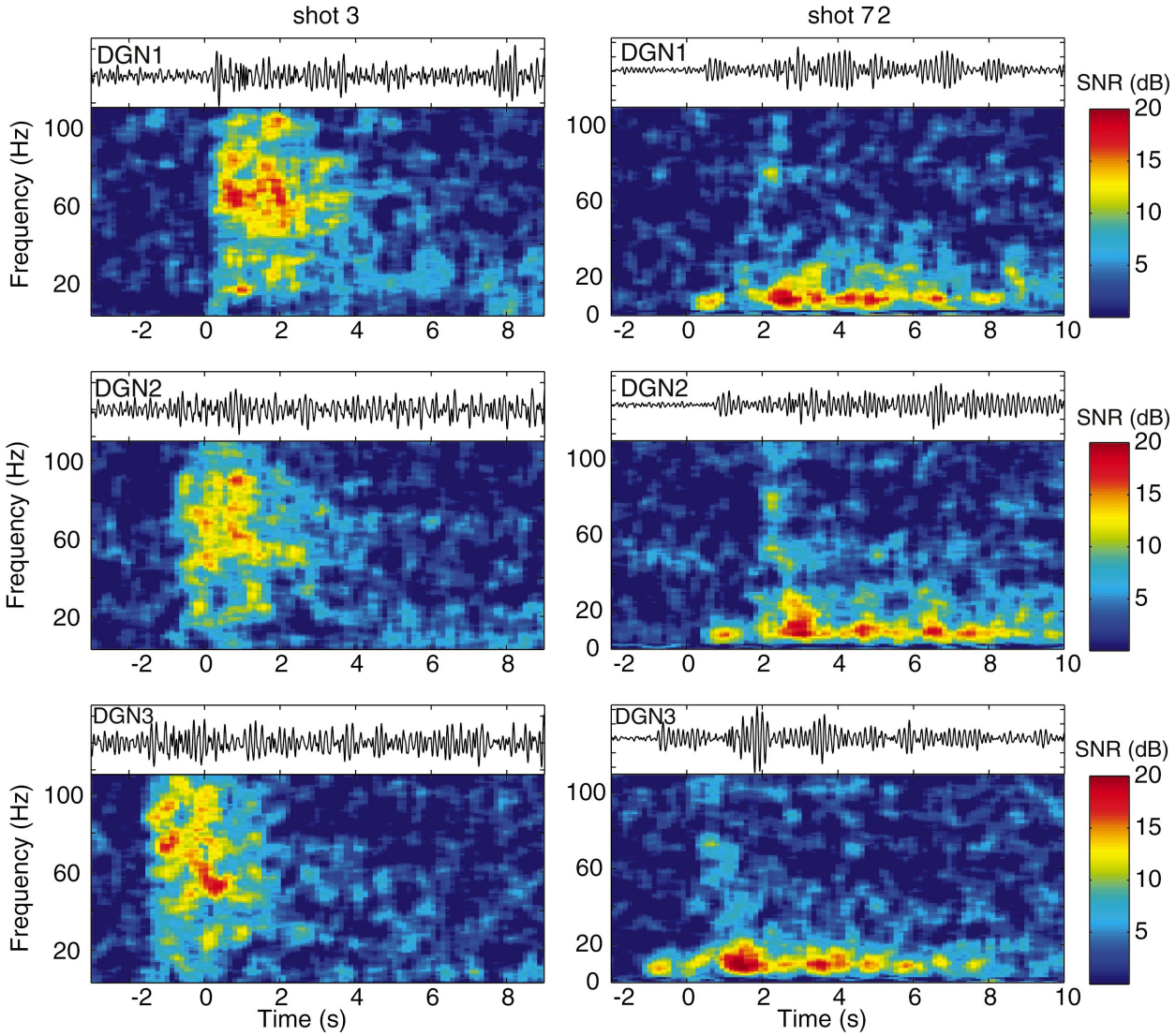

FIG. 7. Examples of individual airgun array shot recordings at the three hydrophones of DGN. Panels on the left show shot 3 from *air1* site. Panels on the right show shot 72 from *air5* site. Unfiltered times series data are plotted above corresponding spectragram in each panel. The spectragrams show signal-to-noise ratio as a function of time and frequency. The spectrum of the signal for each 1 s window is divided by the noise spectrum computed for a 5 s window immediately prior to the shot. Overlap between windows is ~0.9 s.

onset times and solving for the back-azimuths that yield the observed apparent velocity for each hydrophone pair, assuming plane wave propagation. This requires highly accurate time picks because the sensors are so closely spaced. As shown in Fig. 11 for one of the *air5* shots, the initial arrivals at each sensor are highly correlated, so that travel time picks can be made to within 0.05 s. These picks yield a computed back-azimuth with a mean error of 1°, which yields a location uncertainty of 14 km at a distance of 800 km. The later arrivals within the coda are poorly correlated, which suggests that they are being scattered to the receivers along other travel paths. This is consistent with the fact that these shots were located immediately to the east of the Central Indian Ridge (CIR) over a region of complex bathymetry.

The *air9* shot sequence was observed at two stations, which in theory should allow for improved location capability. However, the SNR is too low in the 5–10 Hz band for beam-forming. At higher frequencies, travel time picks cannot be made with sufficient accuracy to make reliable estimates of the apparent velocity, and hence back-azimuths, for either CL or DGS.

Installation of the station at Crozet Island, in 2003, should improve the IMS ability to locate acoustic sources throughout the Indian Ocean. Both the improved triangulation geometry and the added ranging information from the new station will contribute.

V. DISCUSSION

There are three principal methods by which acoustic energy becomes entrained in the oceanic sound channel: direct excitation; downslope propagation; and scattering. Sources near the sea surface, like the airgun shots recorded in this experiment, do not directly excite energy that is channeled between the sea surface and a turning point somewhere above the attenuating seafloor. A very shallow (or very deep) source in the ocean will primarily excite high order acoustic modes that are attenuated due to interaction with the seafloor.

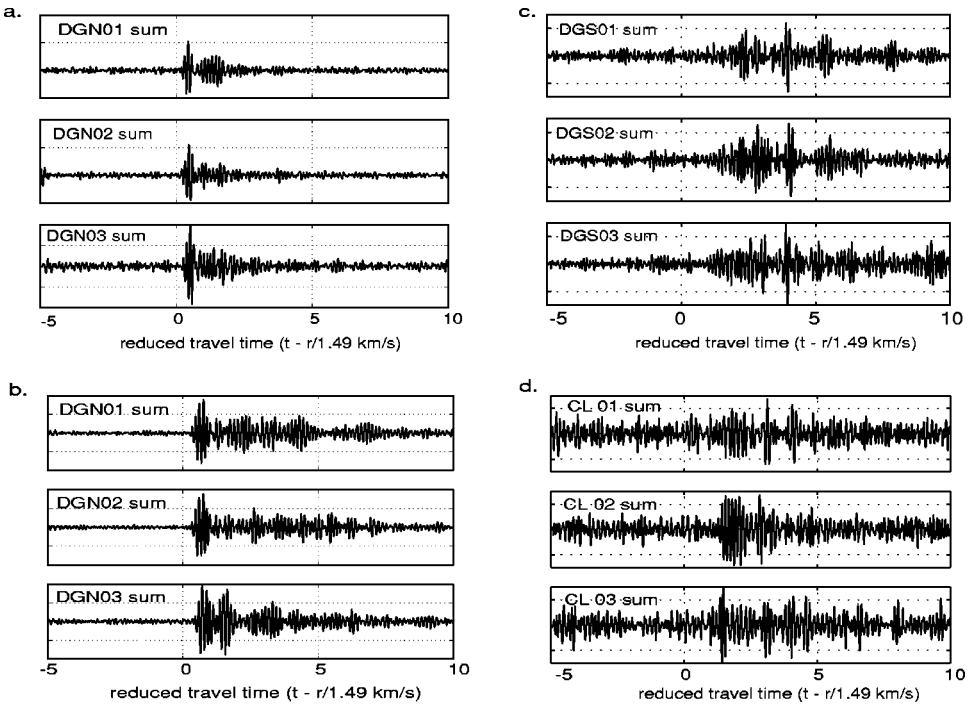

FIG. 8. Examples of airgun array shots recorded at the IMS hydrophones. All shots at each site are stacked after moveout correction. Sections are bandpass filtered 5–10 Hz and time zero corresponds to propagation velocity of 1.49 km/s for each source–receiver range, r. (a) *air2* shots at each of the DGN hydrophones, (b) *air5* shots at the 3 DGN hydrophones, (c) *air9* shots at each DGS hydrophone, (d) *air9* shots at each CL hydrophone.

Some physical process that converts this energy to low order modes that propagate almost horizontally is required. Two mechanisms involving interaction with the seafloor serve to couple high order modes to low order modes, and these are also invoked to describe excitation of acoustic phases, T-waves (Tolstoy and Ewing, 1950), by sub-seafloor sources. These are downslope propagation, which involves repeated interactions of an acoustic phase with a sloping seafloor (Tolstoy and Ewing, 1950), and scattering from a rough seafloor (de Groot-Hedlin and Orcutt, 1999, 2001), which predicts that low order acoustic phases are excited in proportion to the acoustic mode amplitude at the seafloor depth. Thus downslope propagation involves slowly varying bathymetry, while acoustic scattering involves much smaller scale variation in seafloor topography. Park *et al.* (2001) show that T-waves may be excited by a combination of these effects, the key being the occurrence of inhomogeneous structure that enables mode coupling.

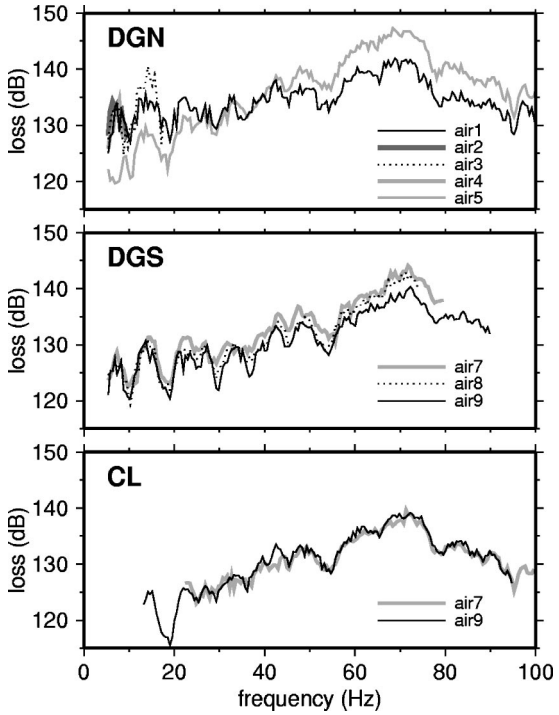

FIG. 9. Transmission loss for each source–receiver pair. The median value of loss for all shots at each site is plotted. Each curve shows only frequencies where signal exceeded current background noise levels by 3 dB. At DGN, *air4* loss is very similar to *air1–air3* losses in the 5–8 Hz band.

Near-source bathymetry was sloped at several of the shooting sites (*air1–air3, air7*). Downslope propagation was a significant factor in coupling high to low order modes. In addition, the T-waves observed in this experiment were probably also excited by scattering of acoustic energy into the sound channel near the source, particularly at *air5*, *air7*, and *air9*. The latter would explain the variability in frequency content of the observed signal between shot sequences, since the amount of scattering depends critically on the roughness scale length in comparison to the acoustic wavelength. This also explains why stacking is ineffective at frequencies above 30 Hz, since even subtle variations in seafloor topography from shot to shot can influence the wave form.

The reason that the *air8* signals were not observed at CL is not certain but topographic variability probably contributes. Kilometer-scale roughness on the eastern flank of the Ninety East Ridge was observed in our swath bathymetry data and these features may scatter energy out of the source–receiver path, thereby reducing the observed signal level for *air8*. The fact that we did observe signals from *air9* probably is due to the existence of a topographic source of coupling just to the south of the shooting site. The slope of Gulden Draak Knoll (Fig. 1) shallows significantly away from our track so this elevated topography could act as a T-wave radiator, both by reflecting direct water waves and through

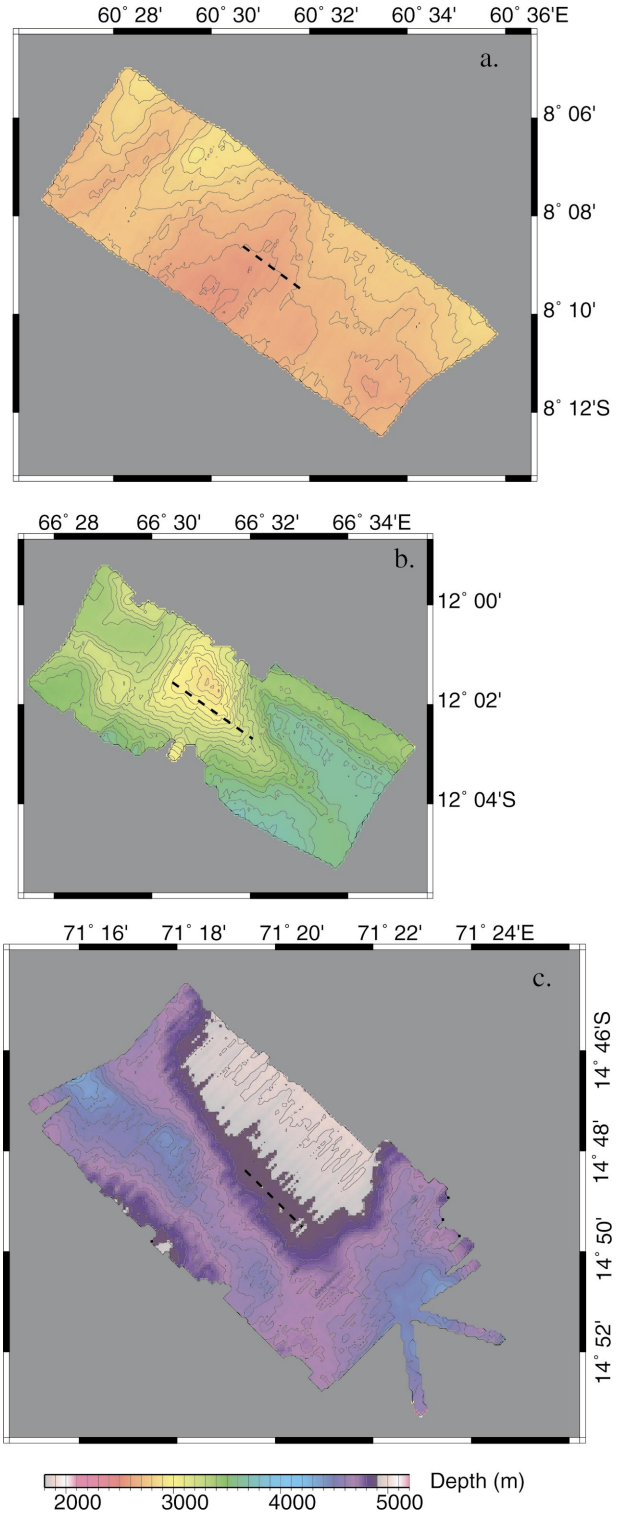

FIG. 10. Hydrosweep bathymetry swaths at representative airgun array shooting sites. Shiptrack runs SE down the center of each swath. Contour interval is 50 m. Coverage shown extends a few kilometers in front of and beyond where the shots were fired (dashed line) to illustrate the broader source region. (a) *air2* site, (b) *air5* site, (c) *air6* site.

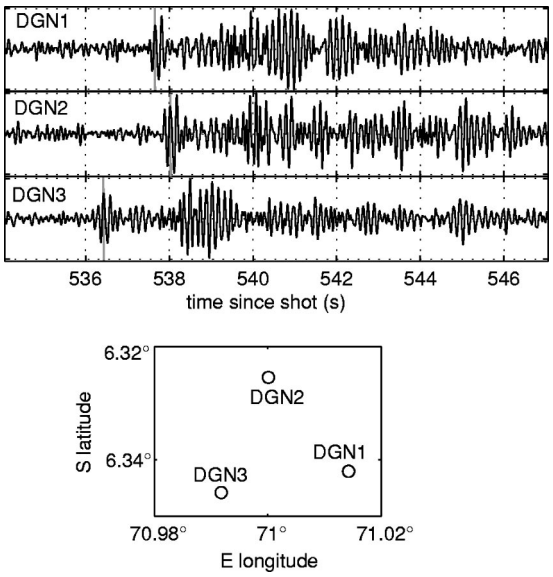

FIG. 11. Arrival time picks for shot 70 (*air5*) used in determining back-azimuth for station DGN. Wave form data for each hydrophone sensor are shown (top) with travel-time pick indicated by gray vertical line. Geometry of the individual sensors at DGN is shown in map view below.

seismoacoustic coupling of crustal waves at the slope, within several kilometers of the shots.

The physical process by which low order acoustic phases are excited has implications for modeling their transmission. Since scattering involves much smaller scale lengths than downslope propagation, much greater detail in the seafloor bathymetry is required in order to accurately model this phenomenon. The Hydrosweep multibeam swath has a sonar footprint on the seafloor that is on the order of 100 m at depths of ~3000 m, thus we could expect to reasonably model T-waves at frequencies up to 15 Hz for very shallow sources with these data. Outside the vicinity of the source the accuracy of the bathymetry required decreases significantly since the T-wave propagates nearly adiabatically after scattering into low order modes.

First-order estimates of acoustic loss for an 8 Hz signal were obtained using a range-dependent, elastic parabolic equation algorithm (Collins, 1993). Acoustic propagation is two-dimensional along the geodesic path from source to receiver, and constant sub-seafloor elastic structure is assumed (Hamilton, 1980; Laske and Masters, 1997). Oceanic properties (Levitus, 1994) and depths (Smith and Sandwell, 1997) varied along the model path. Quantitative comparison between these estimates and our observations (Fig. 9) is not warranted since acoustic energy from shallow sources interacts strongly with the seabed. A seafloor model more precise than is currently available would be required to justify more complete transmission loss modeling for the airgun source. However, the first-order estimates incorporate the effect of broad slopes and overall basin depth variations so we discuss a few qualitative comparisons. The estimated transmission loss at DGN is significant for sites *air6–9* and at DGS the losses for sites *air1–3* are also quite high. Relative loss levels estimated for DGN from sites *air1* and *air2* follow the observed pattern in the 5–10 Hz range. Compared to the *air1* site, a steeper NNE slope characterizes the *air2* site but depths are greater, so less of the energy is reflected toward the sound channel axis. The estimated loss for *air3–5* is greater for DGN than what is observed, most likely due to rough seafloor along the CIR. On the western side of the Ninety East Ridge, *air7* seafloor was characterized by moderate slope at 3400–3700 m. These

depths are well below the axis of the sound channel and the slope geometry was not optimum so that can explain the lack of signal at DGS. However CL, which first-order estimates indicate should have been even less favorable, did record *air7* shots in the 30–60 Hz band. This can be explained by seismic transmission through the crust for several kilometers to the summit of the Ninety East Ridge and subsequent coupling to acoustic modes at the shallower depths near the summit. Current detailed maps (Fisher, 2003) did not indicate the shallowness of the summit of the ridge where our track crossed it; we measured depths as little as 2500 m to the North of our centerbeam.

VI. CONCLUSIONS

At this stage of our investigation, we can conclude that a large airgun array can indeed be used to generate a signal that contains sufficient energy in the 5–60 Hz band to propagate ocean-basin scales (thousands of kilometers). Whether a given hydrophone station will clearly record the signal is a function of background noise levels as well as topographic conditions near the source and along the path to the receiver. At the time of our experiment, noise levels at DGN were favorable, but at DGS and CL the 5–15 Hz band was characterized by background noise that was too high for clear detection of the airgun array shots. However, several of the shots had good SNR in the 30–60 Hz band. A source with greater output than what the airgun array can consistently couple into the sound channel over variable topography would provide a more consistent means of calibrating the Indian Ocean IMS for the lowest (2–15 Hz) frequency band of interest.

The clear recordings of our glass sphere implosions demonstrate that an ocean-basin network characterization using the five-sphere system as a source is possible provided frequency content below 40 Hz is not required. The duration of the signal, even after over 4000 km of propagation, is short and therefore ideal for travel time measurements. At ranges of several hundred kilometers, the single-sphere sources can reliably produce a signal as well, again dominated by frequencies in the upper half of the 2–100 Hz band of interest for nuclear test monitoring.

In areas of shallow, rough topography, it would be necessary to obtain high-resolution bathymetry data to accurately model the higher frequency aspects of the wave form that may contribute to source characterization. The expense of acquiring such data would tradeoff with the level of apparent potential for the region to become a nuclear test site.

ACKNOWLEDGMENTS

This work was supported by DOE Contract Nos. DE-FC03-01SF22356 and W-7405-ENG-48. The captain and crew of the R/V EWING provided excellent shipboard support during the experiment. Bob Fisher kindly provided his most recent version of the Indian Ocean bathymetric compilation. N. Driscoll, F. Sutherland, C. Hollinshead, and J. Stennett made the deployment of the five-sphere glass imploders a reality. C. Keen provided critical logistical support as cruise schedules and shipping requirements changed at the last minute, due to international events of Fall 2001.

[1]At the time of this writing, details on the airgun array and signal were posted at www.ldeo.columbia.edu/Ewing/airguns/ewing_array.html.

Collins, M. D. (**1993**). ''A higher-order energy-conserving parabolic equation for range-dependent ocean depth, sound speed, and density,'' J. Acoust. Soc. Am. **101**, 1068–1075.

de Groot-Hedlin, C. D., and Orcutt, J. A. (**2001**). ''Excitation of T-phases by seafloor scattering,'' J. Acoust. Soc. Am. **109**, 1944–1954.

de Groot-Hedlin, C. D., and Orcutt, J. A. (**1999**). ''Synthesis of earthquake-generated T-waves,'' Geophys. Res. Lett. **26**, 1227–1230.

Fisher, R. L. (**2003**). *GEBCO Digital Atlas—Centenary Ed.*, British Oceanographic Data Centre, Intergovt. Ocean. Comm. and Intl. Hydrogr. Org., Sheet G.08.

Hamilton, E. L. (**1980**). ''Geoacoustic modeling of the sea floor,'' J. Acoust. Soc. Am. **68**, 1313–1340.

Hanson, J., Le Bras, R., Dysart, P., Brumbaugh, D., Gault, A., and Guern, J. (**2001**). ''Operational processing of hydrocoustics at the Prototype International Data Center,'' Pure Appl. Geophys. **158**, 425–456.

Hanson, J. A., Bowman, R., and Beall, G. (**2002**). ''An advanced concept demonstration for monitoring the Indian Ocean,'' Proceedings of 24th Seismic Research Review, pp. 632–642.

Harben, P. E., Boro, C., Dorman, L., and Pulli, J. (**2000**). ''Use of imploding spheres: An alternative to explosives as acoustic sources at mid-latitude SOFAR channel depths,'' University of California Publ. No. UCRL-ID-139032.

Harben, P. E., and Boro, C. (**2001**). ''Implosion source development and Diego Garcia reflections,'' Proceedings of the 23rd Seismic Research Review, pp. 23–31.

Isaacs, J. D., and Maxwell, A. E. (**1952**). ''The ball-breaker; a deep water signaling device,'' J. Mar. Res. **11**, 63–68.

Laske, G., and Masters, G. (**1997**). ''A global digital map of sediment thickness,'' EOS Trans. Am. Geophys. Union **78**, F483.

Lawrence, M. (**2003**). (private communication).

Levitus, S. (**1994**). *World Ocean Atlas 1994*, NOAA Atlas NESDIS 4, Washington D.C.

Orr, M., and Schoenberg, M. (**1976**). ''Acoustic signatures from deep water implosions of spherical cavities,'' J. Acoust. Soc. Am. **59**, 1155–1159.

Park, M., Odom, R. I., and Soukup, D. J. (**2001**). ''Modal scattering: A key to understanding oceanic T-waves,'' Geophys. Res. Lett. **28**, 3401–3404.

Pulli, J., Farrel., T., and Gibson, R. (**1999**). ''Characterization and utilization of hydroacoustic signals reflected from the continent and bathymetric features,'' Procceedings of the 21st Seismic Research Review, pp. 49–56.

Sauter, A. W., and Dorman, L. M. (**2003**). ''Designing a Deep-Towed/Seafloor Repetitive Sound Source,'' EOS Trans. Am. Geophys. Union **84**, Abstract S52D–0163.

Smith, W. H. F., and Sandwell, D. T. (**1997**). ''Global seafloor topography from satellite altimetry and ship depth soundings,'' Science **277**, 1956–1962.

Tolstoy, I., and Ewing, M. W. (**1950**). ''The T phase of shallow focus earthquakes,'' Bull. Seismol. Soc. Am. **40**, 25–51.